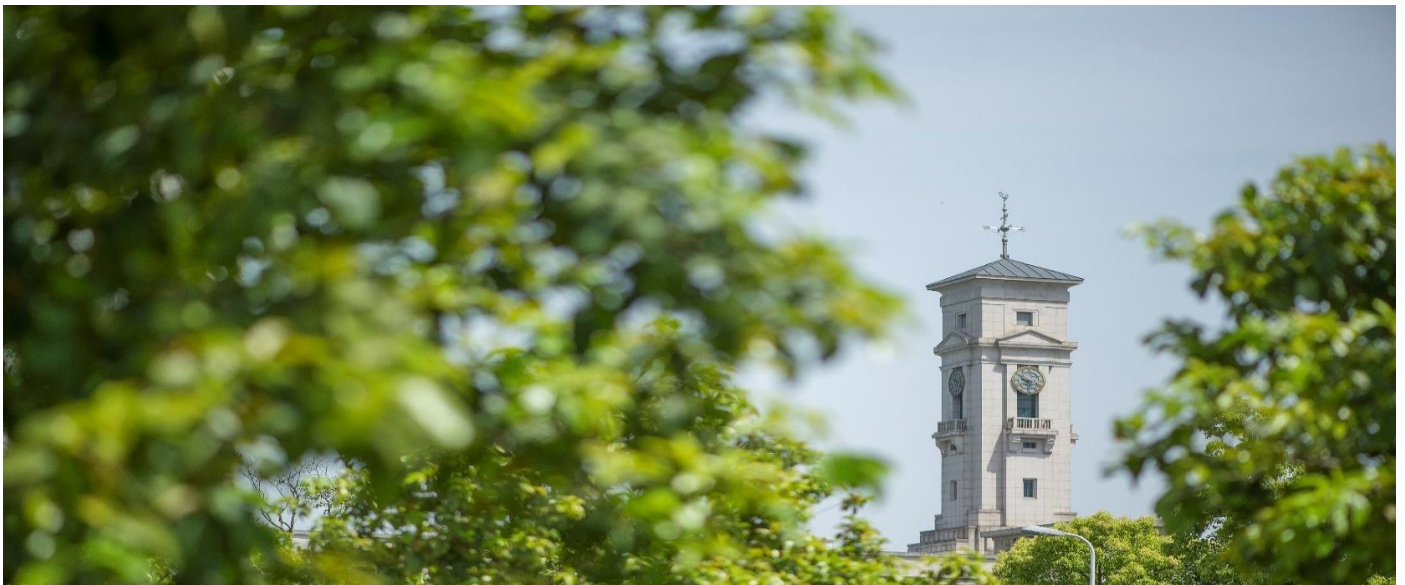


Large-eddy simulation of gas–liquid two-phase flow in a bubble column reactor using a modified sub-grid scale model with the consideration of bubble–eddy interaction

Long, S., Yang, J., Huang, X., Li, G., Shi, W., Sommerfeld, M., Yang, X.



**University of
Nottingham**

UK | CHINA | MALAYSIA

University of Nottingham Ningbo China, 199 Taikang East Road, Ningbo,
315100, China

First published 2020

This work is made available under the terms of the Creative Commons
Attribution 4.0 International License:

<http://creativecommons.org/licenses/by/4.0>

The work is licenced to the University of Nottingham Ningbo China
under the Global University Publication Licence:

[https://www.nottingham.edu.cn/en/library/documents/research-
support/global-university-publications-licence.pdf](https://www.nottingham.edu.cn/en/library/documents/research-support/global-university-publications-licence.pdf)



**University of
Nottingham**

UK | CHINA | MALAYSIA

Large-Eddy Simulation of Gas-Liquid Two-Phase Flow in a Bubble Column Reactor Using a Modified Sub-Grid Scale Model with the Consideration of Bubble-Eddy Interaction

Shanshan Long^a, Jie Yang^b, Xiaobing Huang^c, Guang Li^a, Weibin Shi^{a,d},
Martin Sommerfeld^c, Xiaogang Yang^{a*}

^aDepartment of Mechanical, Materials and Manufacturing Engineering, The University of Nottingham Ningbo China, University Park, Ningbo 315100, PR China

^bSchool of Mathematical Sciences, The University of Nottingham Ningbo China, University Park, Ningbo 315100, PR China

^cFaculty of Arts, Science and Technology, Wrexham Glyndŵr University Wrexham, LL11 2AW United Kingdom

^dCollege of Mechanical Engineering and Automation, Huaqiao University, Xiamen 361021, Fujian Province, PR China

^eFaculty of Process and Systems Engineering, Otto-von-Guericke-Universität Magdeburg, Zeppelinstraße 1, 06130 Halle, Magdeburg, Germany
E-mail: xiaogang.yang@nottingham.edu.cn

Abstract

The Eulerian–Eulerian Large-eddy simulations (LES) of gas–liquid two-phase flow in a cylindrical bubble column reactor have been conducted. When considering the turbulent eddy viscosity in LES, apart from the well-accepted contributions from shear turbulence and bubble induced turbulence (BIT), the effect of the interaction between entrained bubbles and eddies with a similar turbulence length scale to the sub-grid scale (SGS) cannot be neglected. With the consideration of the bubble response to the eddies on the induced sub-grid stresses, a modified SGS model, which incorporates the Stokes number, St , was proposed. The results of LES clearly indicate that the use of the modified SGS model can effectively capture the transient bubbly flow in the cylindrical bubble column. The power turbulent kinetic energy spectrum obtained in LES indicates that a slope similar to Komogorov $-5/3$ scaling law and the -3 scaling law can still be identified for a critical frequency $f=10.70$ Hz.

Keywords: large-eddy simulation; sub-grid scale model; bubble column; turbulence modelling

*Corresponding author: Tel: +86-574-88182419 E-mail: Xiaogang.Yang@nottingham.edu.cn (XY)

1. Introduction

Large eddy simulation (LES) of bubbly flow in bubble column reactors adopts two approaches, which are Eulerian-Eulerian (E-E) and Eulerian-Lagrangian (E-L). The E-L approach adopts the way that the liquid phase momentum equations are solved under the Eulerian frame while the equations for dispersed phase are solved in a Lagrangian framework. The transportation of bubbles is tracked by integrating the bubble motion equation accounting for the forces acted by the liquid phase on the bubbles. A closure model in the liquid and gas momentum equations must be provided to account for liquid-bubble interactions. The bubble size distribution can be calculated as part of the solution at each time step and models are also required to account for break-up and coalescence of the bubbles. However, this kind of approach is quite computationally intensive, thus, it is still inhibitive for studying two-phase bubbly flows in large-scale bubble column reactors or at high void fraction system. As Eulerian-Eulerian two-fluid modelling describes two-phase mixture motion in a macro sense, the use of this approach may be preferable for industrial applications, especially for the case of a highly dispersed void fraction system such as bubble column reactors. The use of Eulerian-Eulerian two-fluid LES modelling is more desirable because the adoption of low order turbulence models, such as the $k-\epsilon$ and even for the Reynolds Stress Model (RSM), may not well capture the instantaneous eddy turbulence structures which will affect the bubble entrainment, breakage and coalescence. Deen *et al.* [1] did pioneering study on LES modelling for gas-liquid flow in a square cross-sectional bubble column. The simulation results were compared with employing the $k-\epsilon$ model. It was concluded that the turbulent viscosity was overestimated by using the $k-\epsilon$ model and only the low frequency unsteady flows could be validated. This is very likely attributable to the transient bubble-eddy interactions being ignored. It has been well accepted that LES can reproduce high frequency experimental data and predict the transient motion of the bubble plume, as experimentally observed. Lakehal *et al.* [2] pointed out that because Reynolds Averaging Navier-Stokes (RANS) models depend on time averaging, they appear to screen out the local fluctuations related to the turbulence as well as the fluctuations related to the interaction between the bubbles and surrounding eddies. However, these local fluctuations are at least partially remained in LES modelling, instead of time averaging, the spatial filtering is employed. It resolves turbulent eddies with the size larger than computational grid directly, while in sub-grid scale (SGS), the behaviour of eddies as well as the interaction between bubbles and the carrier phase are modelled [3]. Furthermore, RANS models are derived by assuming the turbulences are isotropic

in different scale, though the bubbly flows are capable of high anisotropy in velocity fluctuations, especially in the direction of gravity [4]. Conversely, LES modelling only assume isotropy for unresolved scales instead of applying it to resolved scales at the same time.

Less studies have been done on the LES modelling of gas-liquid two-phase flow, which is more challenging, than RANS models. Bombardelli *et al.* conducted simulations of wandering motion in bubble plumes by using both k- ϵ model and LES [5]. The results show that the wandering effect can be reasonably reproduced by employing Smagorinsky SGS model and bubble-slip model, however, the k- ϵ model can only capture the wandering effect at the beginning of the simulation. They also compared both modelling results and indicated that time-averaged axial velocities at different heights above the diffuser for the plane located at mid-thickness by LES still have some discrepancies between the modelling and experimental data. The LES Smagorinsky SGS model has been widely used in recent years, and it has been general practice that the turbulence dissipation introduced by the model is proportional to the Smagorinsky constant, C_S . Deen *et al.* used constant value 0.1 for Smagorinsky constant in the SGS model to simulate the bubbly flow in a bubble column [1] [6], but the sensitivity of the simulation results regarding to C_S is not investigated. It has been accepted that Smagorinsky's eddy viscosity model $\nu_T = (C_S \Delta)^2 |\bar{S}|$, where the model constant C_S can be set to 0.1 is working in the most of single-phase shear flows. However, in subsequent fluid dynamics investigations, researchers have employed this formula directly into two-phase and three-phase flow by changing the model constant from 0.1 to 0.18 empirically, neglecting the multiphase fluid mechanisms behind them. The motivation behind this doing is very likely to consider the change in typical mixing length due to the hybrid effect of the presence of bubbles in the flow. Furthermore, the use of this type of Bossinesq's viscosity model to describe the turbulence energy dissipation in bubbly flow is inappropriate as the bubble wakes also feed the so-called bubble induced turbulence into the flow. Smith and Milelli [7] considered the contribution of bubble induced turbulence into the LES work on liquid phase in bubble plumes, and simulated the dispersed phase by using random dispersion model (RDM). The bubbly flow in a bubble column at low Reynolds number was also simulated by using LES accounting for the effect of bubble induced turbulence by Ma *et al.* [8]. A similar LES modelling for a cylindrical bubble column was conducted by Milelli *et al.* [9] using a relatively coarse cylindrical coordinate grid. They compared both constant and dynamic Smagorinsky SGS model in vertical shear layers

laden with bubbles at very low overall gas hold-up, revealing that the dynamic Smagorinsky SGS model proposed by Germano *et al.* [10] did not have better performance than the constant Smagorinsky model. They also modified the SGS model by taking bubble induced dissipation into account and found that the new SGS model did not remarkably improve the simulation results. It has been revealed by the above researchers that the bubble-induced turbulence model introduced by Sato *et al.* [11] did not have much influence on the turbulent velocity fluctuations in a rectangular bubble column. However, these studies have indicated that the use of the Smagorinsky SGS model with and without considering BIT over-predicted the averaged axial velocity and gas hold up profile. The kinetic energy in sub-grid scale was obtained in a LES work of bubbly flows conducted by Ničeno *et al.* [12]. They derived the turbulent dispersion force as well as the contribution from bubble induced turbulence yielding the transported SGS kinetic energy. They also compared it with the simulation result employing dynamic Smagorinsky SGS model, an improvement was found, but there were still discrepancies with the experimental data. Liu and Li [13] used dynamic Smagorinsky SGS model to simulate the bubbly flow in a bubble column. Different ratios of filter width to bubble diameter were tested to check the mesh independency and the results were compared with the published data. The authors analysed the obtained power spectral density from LES and reported that there exist two zones with slopes of $-5/3$ and $-25/3$, respectively. They claimed that the steep falling off of the slope in the power energy spectrum is due to the BIT as the result of injection of bubbles. Thus, it can be expected that a LES SGS model considering the contribution from BIT in bubbly flow may lead to the simulation results becoming better consistent with the experimental data but depending on how to appropriately consider the BIT. It should be pointed out that the turbulent viscosity model accounting for the BIT in two-phase flow as proposed by Sato and Sekoguchi [14] was derived by assuming the flow about a fixed bubble as the flow about a cylinder. In reality, the bubbles will response to the turbulent eddies that entrain the bubbles. This response should exist at the sub-grid scale where the bubbles may not follow the turbulent eddy motion faithfully. When assessing this type of bubbles' dynamic response to eddies, one can consider the slip velocity between the bubbles and eddies to be influenced by the response of the bubbles to eddies. The bubbles appear to escape from the turbulent eddies where they are entrapped because of the buoyancy effect. Therefore, the instantaneous fluctuation of bubbles would always differ from it of the surrounding turbulent eddies in sub-grid scales, especially for the eddies having the similar size with the bubble diameter

[15]. Secondly, in bubbly flow, the interfacial forces acting on the bubbles are strongly influenced by the interactions between the bubbles and the near eddies, and these forces have to be properly implemented in LES SGS modelling. In addition, the bubbles that rise in the bubble column will encounter those turbulent eddies generated by the shear turbulence and the preceding bubble wakes in their paths. The relative size difference between bubbles and eddies lead to different relaxation times. Therefore, the instantaneous filtered velocity of a bubble is strongly correlated to the turbulent eddy fluctuation velocity.

It should be mentioned here that bubble size distribution has a pivotal role in predicting gas-liquid interfacial area, which will further influence the prediction of the mass and heat transfer between phases. To obtain the bubble size distribution when using the E-E approach, additional equations accounting for bubble breakup and coalescence, together with bubble growth or shrinkage because of mass transfer are required. Studies on the bubble size distribution in various bubbly flows can be found in the literature. Different models derived from population balance equation were developed, such as the multiple size group model (MUSIG) [16], the interfacial area transport models [17-21]. When using the E-E modelling approach for practical applications [22], the dispersed bubbles are treated as a quasi-continuum with each computational grid in whole domain containing corresponding fractions of the carrier and dispersed phases. Separate momentum and continuity equations are solved together on the same grid for each phase. For LES, by applying the filtering at a filter scale (Δ), the filter scale should fall into the inertial sub-range region in turbulent kinetic energy spectrum as a key criteria for a successful E-E LES as indicated by Niceno *et al.* [12], and thereby the scale of motion greater than Δ can be resolved. However, it is noticeable that the bubble-induced large scale turbulent eddies with the size larger than Δ cannot be resolved properly in LES, due to the missing information of interphase details above filter scale. In addition, bubble-induced turbulence not only affects the carrier phase liquid flow for the length scale smaller than bubbles but also has the impact on the large scale flow as reflected in the predicted turbulent kinetic energy spectrum obtained from the LES modelling. This may deteriorate the accuracy of predicting the resolved scale motion of the large eddies in LES. Thus the grid requirements may sometimes be in confliction when modelling with the E-E LES. Milelli [23] has proposed the requirement of grid size in the E-E LES and carried out a parametric investigation on different mesh resolutions and bubble diameters. It was suggested that $1.2 < \Delta/d_B < 1.5$ ($0.67 < d_B/\Delta <$

0.83) would be an optimum filter width [24]. The comparative study was conducted by Dhotre et al. [4] for $\Delta/d_B = 1.2$ and 2.5, and they found that good agreement with the experimental data can be still obtained for both grids. Niceno et al. [12] has trialed a grid refinement study on $\Delta/d_B = 1.25$ and 2.5 but demonstrated similar quantitative vertical gas and liquid velocity to be shown by applying both grids. Liu and Li [13] also employed the E-E LES model with 5 different Δ/d_B in their study on bubble column bubbly flows and have revealed that the adoption of the ratio of grid to bubble size $\Delta/d_B = 1.25$ and 1.5 can yield the results agreed with the experimental results. Generally speaking, the application of $\Delta/d_B > 1.0$ for the E-E LES modelling is required based on the previous studies mentioned above. It should be noted that the E-E LES modelling of bubbly flows accounting for the bubble size distribution coupled with for bubble coalescence and breakage is still rarely reported, to the best knowledge of the authors.

This work aims to implement a modified Smagorinsky SGS model which accounts for the bubble response to the surrounding turbulent eddies through introducing a Stokes number into the LES simulation of a cylindrical bubble column. The mathematical modelling and numerical methods are presented in Section 2. The simulation results and related discussion will be then followed in Section 3, focusing on the effect of bubble response to the turbulent eddies in SGS scale and the BIT influence on the simulated turbulent kinetic energy power spectrum together with the correlations between the turbulent eddy structures and bubble distribution in the bubble column. Finally, this paper will end with a conclusive summary of key findings.

2. Mathematical modelling and numerical methods

2.1 Governing equation

The LES model is obtained by spatially filtering the equations of momentum. The current study employs a Eulerian-Eulerian two-fluid model with each phase being described by separate equations. For phase k , the filtered equations of mass and momentum can be expressed by Equations (1) and (2),

$$\frac{\partial}{\partial t}(\rho_k \alpha_k) + \nabla \cdot (\alpha_k \rho_k \mathbf{u}_k) = 0 \quad (1)$$

$$\frac{\partial}{\partial t}(\alpha_k \rho_k \mathbf{u}_k) + \nabla \cdot (\alpha_k \rho_k \mathbf{u}_k \mathbf{u}_k) = -\nabla \cdot (\alpha_k \boldsymbol{\tau}_k) - \alpha_k \nabla p + \alpha_k \rho_k \mathbf{g} + \mathbf{M}_{F,k} \quad (2)$$

where $k = G$ and $k = L$ represents for gas and liquid respectively. The terms on the right-hand side of Equation (2) stand for the contributions due to the stress, the pressure gradient, gravity and momentum exchange between each phase that arise from the actions from interfacial forces individually. The stress term can be defined by Equation (3),

$$\tau_k = -\mu_{eff} \left(\nabla \mathbf{u}_k + (\nabla \mathbf{u}_k)^T - \frac{2}{3} I (\nabla \cdot \mathbf{u}_k) \right) \quad (3)$$

where μ_{eff} represents the effective viscosity for the continuous phase, which may be assumed to be consisted of the following terms: the molecular viscosity μ_L , the turbulent viscosity μ_T and an additional term to describe bubble induced turbulence μ_{BI} [4]. This is defined in Equation (4).

$$\mu_{eff} = \mu_{L,L} + \mu_{T,L} + \mu_{BI,L}. \quad (4)$$

The bubble induced turbulence can be modelled based on Sato's model [11], which is given by Equation (5).

$$\mu_{BI,L} = \rho_L C_{\mu,BI} \alpha_G d_B |\mathbf{u}_G - \mathbf{u}_L|. \quad (5)$$

The momentum exchange term that introduces the interface forces is defined by Equation (6),

$$\mathbf{M}_{F,L} = -\mathbf{M}_{F,G} = \mathbf{M}_{D,L} + \mathbf{M}_{L,L} + \mathbf{M}_{TD,L} + \mathbf{M}_{AM,L} \quad (6)$$

where the terms including, from left to right, the interface drag force, lift force, turbulence dispersion force and virtual mass force, respectively.

Drag force

The interphase momentum transfer between continuous and dispersed phases because of the drag force contributed from both viscous shear (skin drag) and the pressure gradient (form drag) can be expressed by Equation (7),

$$\mathbf{M}_{D,L} = \frac{3}{4} \alpha_G \rho_L \frac{C_D}{d_B} |\mathbf{u}_G - \mathbf{u}_L| (\mathbf{u}_G - \mathbf{u}_L) \quad (7)$$

where the drag coefficient, C_D , can be expressed by using Equation (8) with regard to distorted bubbles [25],

$$C_D = \frac{2}{3} E_0^{\frac{1}{2}} \quad (8)$$

where the Eötvös number $E_0 = \frac{g \Delta \rho d_B^2}{\sigma}$ stands for the ratio of the buoyancy to the surface tension forces.

Lift force

Due to the radial velocity gradient in the bubble column, the lift force acts on the rising bubbles perpendicularly to the relative motion of gas and liquid phases. The correlation between slip velocity and the curl of liquid velocity is associated with the lateral lift force [26, 27], which is given by

$$\mathbf{M}_{L,L} = \rho_L C_L (\mathbf{u}_B - \mathbf{u}_L) \times (\nabla \times \mathbf{u}_L) \quad (9)$$

where C_L is the lift force coefficient and is based on the estimation according to Tomiyama *et al.* [28] by

$$C_L = \begin{cases} \min[0.288 \tanh(0.121 Re_B), f(E'_0)] & E'_0 \leq 4 \\ f(E'_0) & 4 < E'_0 < 10 \\ -0.29 & E'_0 > 10 \end{cases} \quad (10)$$

where Re_B is the bubble Reynolds number and $E'_0 = \frac{g(\rho_l - \rho_g)d_h^2}{\sigma}$, $d_h = d(1 + 0.163E_0^{0.757})^{1/3}$.

Added mass force

The relative acceleration of the bubble and surrounding liquid is considered by the added mass force [29], which can be estimated by

$$\mathbf{M}_{AM,L} = \alpha_G \rho_L C_{AM} \left(\frac{D\mathbf{u}_G}{Dt} - \frac{D\mathbf{u}_L}{Dt} \right) \quad (11)$$

where C_{AM} stands for the virtual mass coefficient and a constant 0.5 is used through this paper.

Turbulent dispersion force

Considering the effect of the random fluctuations of turbulent eddies, the turbulent dispersion force is considered in the current simulation. The formulation proposed by Burns *et al.* [30] to estimate the force is adopted, given by

$$\mathbf{M}_{TD,L} = C_{TD} \frac{3\alpha_G \rho_L}{4 d_B} (\mathbf{u}_L - \mathbf{u}_G) \frac{\nu_t}{\sigma_{TD}} \left(\frac{\nabla \alpha_L}{\alpha_L} - \frac{\nabla \alpha_G}{\alpha_G} \right) \quad (12)$$

where C_{TD} is the turbulent dispersion coefficient and is assumed to constant 1 in this work, ν_t is the turbulent kinematic viscosity and σ_{TD} represents the turbulent Schmidt number, $\sigma_{TD} = 0.9$ is adopted here.

In LES, the velocity in Equations (1) and (2) are described by Equation (13),

$$\mathbf{u}_k = \tilde{\mathbf{u}}_k - \mathbf{u}'_k \quad (13)$$

where \mathbf{u}_k is the velocity that needs to be resolved in filtering, while $\tilde{\mathbf{u}}_k$ represents the instantaneous velocity and \mathbf{u}'_k stands for the unresolved part that requires the closure from the use of the SGS model in the LES simulations. It needs to be noted that the equations of mass and momentum are derived by time-averaging in RANS models. In LES modelling, these equations are solved by spatial filtering, hence, $\tilde{\mathbf{u}}_k$ and \mathbf{u}'_k are referred to grid scale and sub-grid scale velocity, respectively.

Following Garcia's work [31] but considering the contribution from the added mass on bubble translation, the relative velocity between the carrier fluid and the bubble can be obtained from Equation (14),

$$\mathbf{u}_\lambda \sim \frac{(\varepsilon\lambda)^{\frac{1}{3}}}{\left(1 + \frac{1}{2} \frac{C_D \rho_L S}{(\rho_B + C_{AM} \rho_L) V} \lambda\right)^{\frac{1}{2}}} \quad (14)$$

where λ represents the different turbulent length scales in the range between the integral and Kolmogorov scales ($L > \lambda > \eta$) and C_{AM} is the added mass coefficient. When the derivative of u_λ equals zero at a certain λ , u_λ will have a maximum, as defined by Equation (15).

$$\lambda^* \sim \frac{4(\rho_B + C_{AM} \rho_L) V}{C_D \rho_L S} \quad (15)$$

Substituting λ^* into Equation (14) yields

$$\mathbf{u}_\lambda^* \sim (\varepsilon d)^{\frac{1}{3}} \left(\frac{1}{C_D}\right)^{\frac{1}{3}} \left(\frac{\rho_B + C_{AM} \rho_L}{\rho_L}\right)^{\frac{1}{3}} \quad (16)$$

In this turbulent length scale range, $(d\varepsilon)^{1/3}$ can be regarded as the fluctuating velocity of the bubble. Thus, \mathbf{u}_λ^* can be expressed as,

$$\mathbf{u}_\lambda^* \sim \mathbf{u}'_G \left(\frac{1}{C_D}\right)^{\frac{1}{3}} \left(\frac{\rho_B + C_{AM} \rho_L}{\rho_L}\right)^{\frac{1}{3}} \quad (17)$$

The size of the bubbles and their surrounding turbulence eddies are different, hence, bubbles will not respond immediately to the flow motion of the eddies. Taking their slip velocity into account, the bubbles appear to get rid of the controlling from the eddies where they are entrapped [32]. As demonstrated in Equation (18), the instantaneous fluctuation of bubbles would always be smaller than the surrounding turbulent eddies' fluctuation in sub-grid scales, especially for the eddies having the similar size with the bubble diameter. Considering the modified bubble equation of motion with the Stokes number and the interaction between bubbles and eddies, the Smagorinsky model of sub-grid eddy viscosity can be modified for the case where the drag force can be regarded as the dominant acting force. According to Kruijs and Kusters [15], the correlation between the

fluctuating velocity of bubble and liquid in terms of the turbulent eddies with length scales in the inertia subrange can be expressed by Equation (18).

$$\frac{u_G'^2}{u_L'^2} = \frac{1}{1+St} \quad (18)$$

When Equation (18) is implemented into the sub-grid scale, the relationship can be defined as

$$\frac{u_G'^2}{u_{L,SGS}'^2} = \frac{1}{1+St_{SGS}}, \text{ where } St_{SGS} \text{ is the non-dimensional Stokes number given by } St = \frac{\tau_{\text{bubble}}}{\tau_{L,SGS}}. \text{ Here,}$$

the bubble response time scale is proposed by Sommerfeld *et al.* [33], $\tau_{\text{bubble}} = \frac{4(\rho_G+0.5\rho_L)d_B^2}{3\mu_L C_D Re_B}$. In

terms of liquid response time in SGS, $\tau_{L,SGS} = \Delta/u_{L,SGS}'$, where $\Delta = (\Delta_i \Delta_j \Delta_k)^{1/3}$ is the filter width and $u_{L,SGS}'$ stands for the liquid velocity in local grid.

As $u_L'^2 \sim (\lambda \varepsilon)^{2/3}$, one can obtain Equation (19) which is given by

$$u_\lambda^* \sim \left(\frac{1}{1+St_{SGS}} \right)^{\frac{1}{2}} (\lambda \varepsilon)^{\frac{1}{3}} \left(\frac{1}{C_D} \right)^{\frac{1}{3}} \left(\frac{\rho_B + C_{AMPL}}{\rho_L} \right)^{\frac{1}{3}} \quad (19)$$

The turbulence dissipation due to the bubbles corresponds to the inertial subrange can be assumed that mainly occurs when λ approach to λ^* , and the dissipation can be estimated by Equation (20).

$$-\tau_{ij} \overline{S_{ij}}|_G \sim \rho_L C_D \left(\frac{\rho_L}{\rho_B} \right) \frac{u_\lambda^3}{d_B} \overline{\alpha_G} = C_b \rho_L \varepsilon \overline{\alpha_G} \frac{\lambda}{d_B} \left(\frac{1}{1+St_{SGS}} \right)^{\frac{3}{2}} \quad (20)$$

Different values of the constants C_b have been trialled, but a value of 0.7 is employed which demonstrates good agreement with Camasara's results. $\overline{\alpha_G}$ stands for the local gas hold-up after filtering. The total dissipation is given by Equation (21).

$$-\tau_{ij} S_{ij} \sim \rho_L \varepsilon \left(1 + C_b \overline{\alpha_G} \frac{\lambda}{d_B} \left(\frac{1}{1+St_{SGS}} \right)^{\frac{3}{2}} \right) \quad (21)$$

Employing the eddy viscosity model, the liquid-phase turbulence modified SGS viscosity can be modified as represented by Equation (22),

$$\mu_{T,L} = \rho_L (C_s \Delta)^2 |S| \left(1 + C_b \overline{\alpha_G} \frac{\Delta}{d_B} \left(\frac{1}{1 + St_{SGS}} \right)^{\frac{3}{2}} \right) \quad (22)$$

where C_s is the Smagorinsky constant and S represents the characteristic resolved strain rate tensor. λ has been assumed as the filter length scale Δ in the range of the inertia subrange.

2.2 Numerical Modelling

In order to demonstrate the reliability of the proposed modified LES SGS model, the simulation of bubbly flow in the bubble column reactor, based on the work of Camarasa *et al.* [34] and Kulkarni *et al.* [35], have been carried out. The experimental settings are summarized in Table 1. Based on Camarasa's experimental work, a distributor containing 62 holes that are 1 mm in diameter was evenly placed at the bottom of the bubble column. Based on Kulkarni's work, air was sparged through a 20 μm perforated plate using an oil-free diaphragm compressor.

Table 1. Details of experimental set-up

Experiments conducted	Diameter (m)	Height (m)	Superficial gas velocity (m/s)	Static liquid height (m)	Observation position (m)
Camarasa <i>et al.</i> [34]	0.1	2	0.0372	0.9	0.6
Kulkarni <i>et al.</i> [35]	0.15	1.5	0.0382	0.65	0.3

The solver of ANSYS CFX 18.0 was employed in the LES simulation. At inlet, a mass flow rate condition normal to inlet was used. In the current work, the inlet mass flow rate is given by $\dot{m} = \rho_g A_D v_g$, and the volume fraction for liquid and gas phases are specified as $\alpha_L = 0$ and $\alpha_G = 1$. The bubble diameter of 4 mm is adopted in this work, which is the typical value of gas-liquid bubble columns under the same pressure, superficial velocities and air-inlet distributor conditions. At the top surface of the bubble column, a pressure-constant boundary (relative pressure of 0) is applied. No slip condition is employed for the wall. It should be noted that the bubble size will

increase along the height of bubble columns and this change in bubble size is usually very small, thus leading to the negligence of such change in the numerical simulation, certainly in the currently available reported studies using Eulerian-Eulerian LES [1,3,44,12,13,58]. According to Zhao's *et al.* study on evolution of bubble size distribution from gas blowout in shallow water [59], the compressibility factor can be used for characterisation of bubble size changes with liquid depth. By approximating of the cases of bubble column bubbly flows, the variation of the compressibility factor z for bubble size along a stationary liquid level height of 0.9m in the bubble column is very marginal. Also, the bubble rise-up in a stationary water tank is considered as an example. Assuming that the water level height is 0.9 m and the ambient pressure to be 1 bar, one can roughly use the equation of status to estimate the bubble diameter for the bubble to just reach the surface of the water if a bubble is released from the bottom of the tank with an initial diameter of 4 mm, which only yields 4.11 mm. It can be seen clearly that the percentage of the diameter increment for the bubble released from the sparger of the bubble column is approximately 3%. Accordingly, the bubble size change with the local pressure along the bubble column height can be disregarded if no bubble breakup or coalescence takes place and bubbly flow is dilute.

A central differencing scheme is implemented for the discretisation of the advection term, while a second-order backward Euler scheme is used for the time discretisation in the simulations. Employing an Eulerian-Eulerian approach and the LES model, the bubble column was discretised with uniform $\Delta x^+ = 100$ and $\Delta r^+ = 5$ with a growth rate of 1.5 in the region near the wall. Three grids were used in the central region of the bubble column in the current work: $d_B/\Delta = 0.57, 0.75, 0.9$ with globally 1,778,700 mesh elements in the finest grid and 5,344,600 in the coarsest one. The mesh set-up of $d_B/\Delta = 0.75$ in the central region is shown in Fig. 1. The corresponding grid resolution study regarding the modified SGS model is presented in next section.

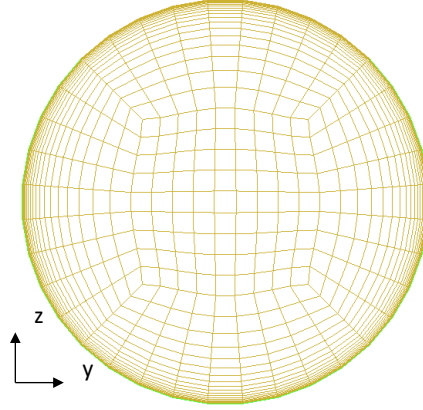


Figure 1. Cross section of the mesh set-up ($d_B/\Delta = 0.75$) in the bubble column.

3. Results and Discussion

The gas-liquid flow in the bubble columns have been simulated using a constant time step size of 0.001 s for resolving the temporal variations of the flow field. Since the bubbly flow in the bubble column is transient, the simulation was run for 100 s and the data was collected over the last 50 s until the turbulent flow field becomes statistically stationary. The results and findings based on the simulations are discussed as follows.

3.1 Grid independency study

In this section, the results obtained on various d_B/Δ values from 0.57 to 0.9 were compared with the published experimental data by Camarasa *et al.* [33]. Figure 2 (a) and (b) shows the comparisons of time-averaged gas velocity and gas hold-up at $H/D=6$. The velocity and gas hold-up was calculated by collecting the instantaneous velocity at different positions along the radius of bubble column between 50 s and 100 s using the ensemble averaging (equivalent to time averaging) method. The time-averaged velocities are obtained by using the following relation:

$$\bar{u}_B(r) = \frac{1}{N\Delta t} \sum_{i=1}^N \mathbf{u}_{Bi}(r, t)\Delta t \quad (23)$$

where \bar{u}_B is the average bubble velocity, N is the sampling number for collection of the instantaneous bubble velocity at the given radial position and Δt is the time step for the simulation.

It can be seen from the figure that the LES results using three grids generally follow up the trend of the experimental axial gas velocity. One can observe that there is not significant difference in the predicted axial velocity profiles for the grids of $d_B/\Delta=0.75$ and slightly refined mesh $d_B/\Delta=0.9$. The results of both the two grids are in good agreement with the experimental data compared with the result obtained by using the coarse mesh $d_B/\Delta=0.57$. In Figure 2(b), the time-averaged gas hold-up is obtained by using the following expression:

$$\alpha_{Gcross}(H) = \frac{1}{\pi R^2} \int_0^R \left(\frac{1}{T_1 - T_0} \int_{T_0}^{T_1} \alpha_G(r, H, t) dt \right) 2\pi r dr \quad (24)$$

where T_0 and T_1 are the beginning and end time for sampling. As can be seen the figure that the predicted gas-holdup profiles using all three different grids have higher values in the range of large r/R but there is only tiny difference in the predicted gas holdup profiles using the meshes of $d_B/\Delta=0.75$ and 0.9 . Further detailed discussion and comparisons on the simulations using the standard Smagorinsky SGS and the proposed modified SGS model will be presented in Section 3.2. It can be seen from the comparisons that compared with the results obtained using the coarse mesh $d_B/\Delta=0.57$, the simulations using $d_B/\Delta=0.75$ and 0.9 do give better prediction on the axial gas velocity and air void fraction, consistent with the experimental ones. With caution, $d_B/\Delta=0.75$ has been adopted in the present E-E LES modelling (around 1,200,000 mesh elements in total were adopted, especially in the center region of the bubble column. It should be noted here that this grid resolution is consistent with the condition used in Milelli's work [23] and it is expected that the turbulence with the scale being larger than the bubble diameter can be well resolved.

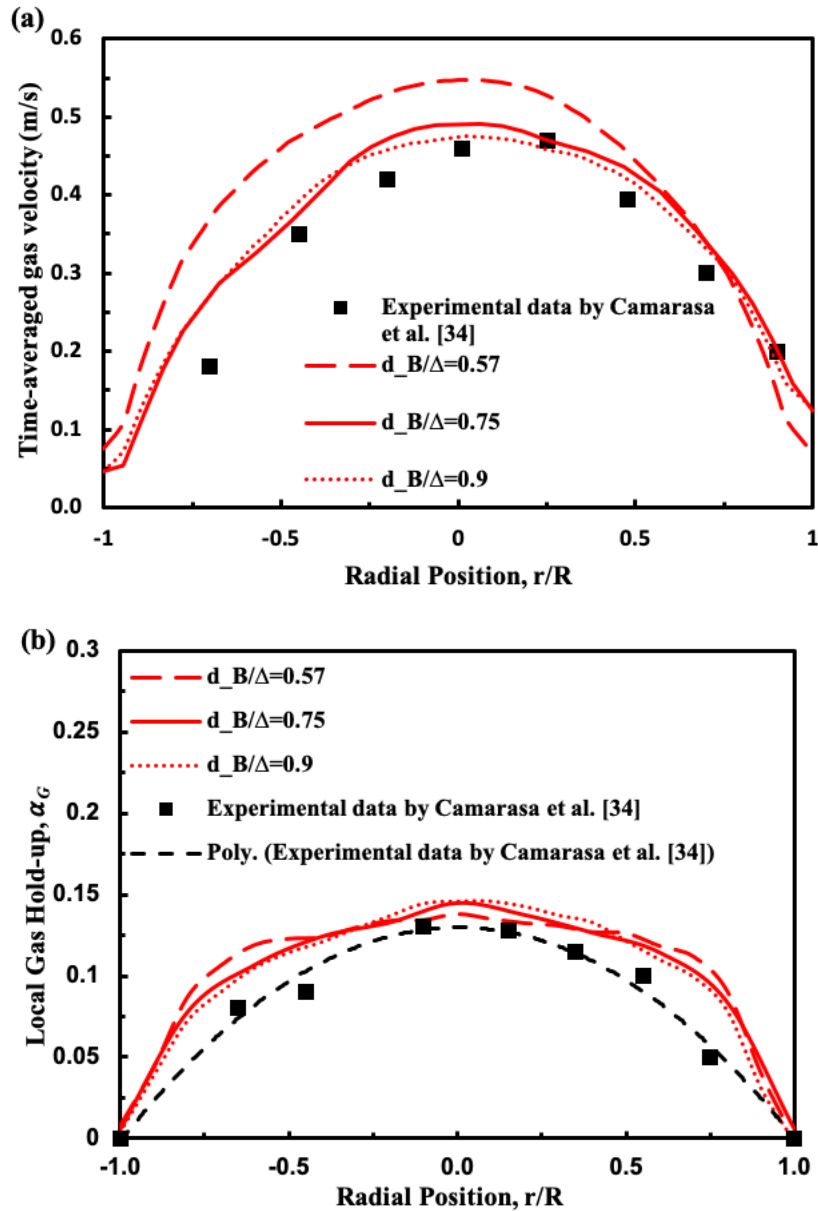


Figure 2. Time-averaged (a) axial gas velocity and (b) radial distribution of gas hold-up at $H/D=6$ obtained on three grids, and experiments [34].

3.2 Predicted flow patterns, gas holdup and velocity distributions

Chen *et al.* [36] have indicated that the bubbly flow in bubble columns consists of four flow regions including descending flow region, vortical-spiral flow region, fast bubble region and the central plume region. It is shown in Figure 3 that the LES simulation implemented the modified SGS model has well captured the features of vortical-spiral upward bubbly flow in the bubble column.

As illustrated in Figure 3, the flow patterns for the flow time of 3.78, 50.0, 75.0 and 90.0 s, displayed with instantaneous velocity vectors based on instantaneous gas hold-up, clearly exhibits bubbles spirally rising-up. The descending flow can be observed to take place near the wall in the form of the downward velocity vectors pointing downwards, while the higher gas hold-up at the central region of the bubble column indicates that the bubbles are clustered and entrained by large eddies that rise up in the centre of the bubble column. At $t = 3.78$ s, the vortical-spiral flow is not yet fully established while at $t = 50.0, 75.0$ and 90.0 s, it can be found from Figure 3 that a large amount of large vortices are oscillating throughout the bubble column, accompanied by the numbers and distributions of large eddies that fluctuate with time and position.

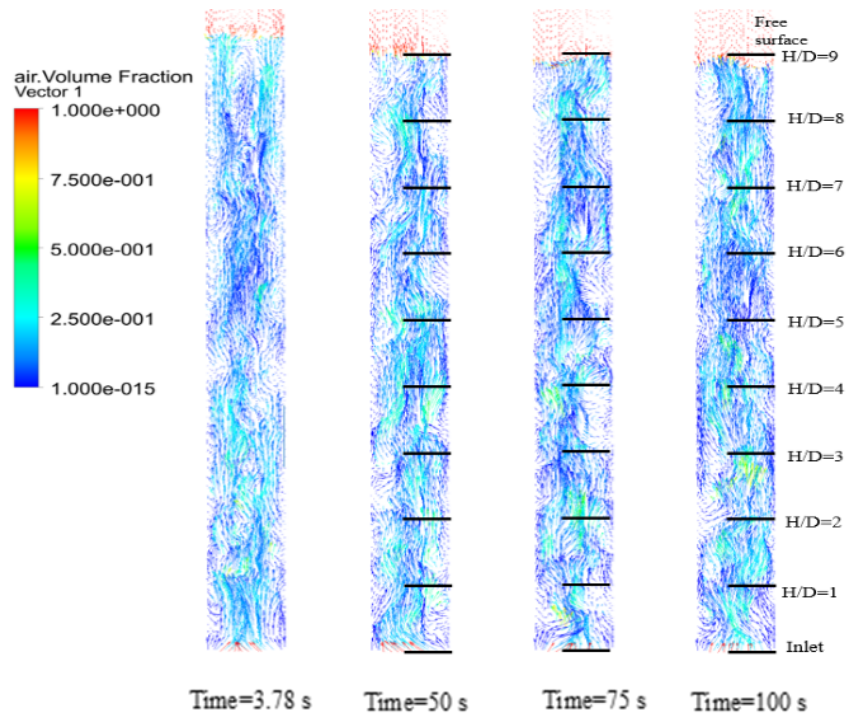


Figure 3. Snapshots of LES simulated instantaneous velocity vectors highlighted by gas hold-up distribution.

In Figure 4, the averaged bubble and liquid velocity profiles at $H/D = 6$ obtained by applying both the modified SGS and standard Smagorinsky SGS models are presented. By applying the same method as evaluated using Equation (23), a quantitative comparison is made with the published experimental data obtained by Camarasa *et al.* [34]. It can be shown from Figure 4 that the averaged bubble axial velocities obtained from the LES with the modified SGS model are in good

agreement with the experimental results [34], remarkably improved in comparison to the use of standard SGS Smagorinsky model. However, such consistency becomes poor close to the column wall. A likely reason is that the interaction between bubbles and turbulent eddies may be not well reflected in the modified SGS model as the bubble size is greater than the grid size. In terms of the grid set-up employed in the present simulation, Milelli's condition is only held in the central part of the bubble column, while d_B/Δ close to the wall region is much larger than 0.75 [27]. This causes a relative poor performance of the modified SGS model in the estimation of the eddy viscosity in the region near the wall. However, as LES imposes the requirement of $5 < r^+ < 10$, the use of Milelli's condition will violate this constraint. This remains for further investigation.

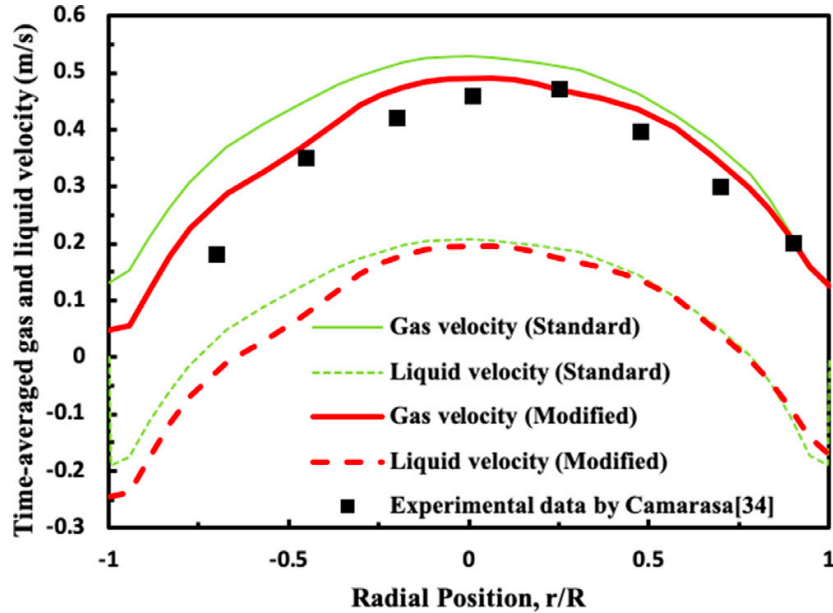


Figure 4. Time-averaged axial gas and liquid velocity at $H/D=6$ (Green line: standard Smagorinsky SGS model; Red line: Modified Smagorinsky SGS model; Solid line: Gas; Dashed line: Liquid).

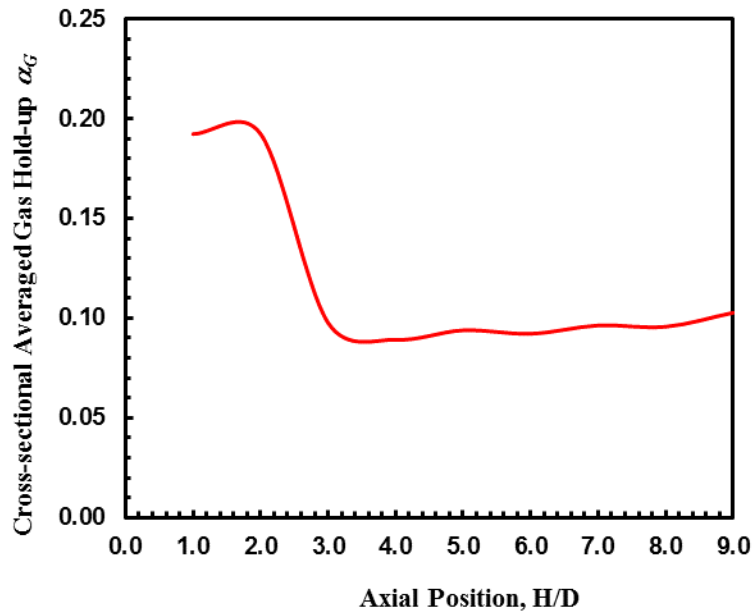


Figure 5. Time-averaged axial distribution of gas hold-up at centerline.

Figure 5 shows the cross-sectional averaged gas hold-up variation along the bubble column height after time-averaging, which can be obtained by using Equation (24). As can be seen from Figure 5 that the averaged gas hold-up is decreasing with the increasing of the axial height for the region where the bubble rise-up is close to the gas distributor at the inlet. The released bubbles from the distributor have not achieved the sub-steady spiral rise-up status. The bubbles are strongly affected by the recirculation large vortices near the inlet, which result in a significant fluctuation in the simulated bubble volume fraction. After the flow reaches a certain height, the bubble entrainment becomes relatively steady, yielding a result of the bubble volume fraction being almost unchanged along the height. It appears that the bubbly flow in the bubble column for present study condition can be divided into two regions where the characteristics of bubble volume fraction can either change significantly or less significantly. The two regions are separated at approximately $H/D = 2.5$.

The time-averaged gas holdup distribution at $H/D = 6$ in the radial direction is presented in Figure 6. It can be obtained that the simulation is quantitatively consistent with the experimental data as reported in Camarasa's *et al.* work [34]. It should be noted, however, that the profile of the averaged gas hold-up by LES is over-predicted for the location between the column wall and core region. One explanation is that the inhomogeneity which causes bubble induced turbulence during

the ascending recirculation flow near the bubble column wall is not well reflected by the proposed modified SGS model in the present LES. This requires further investigation.

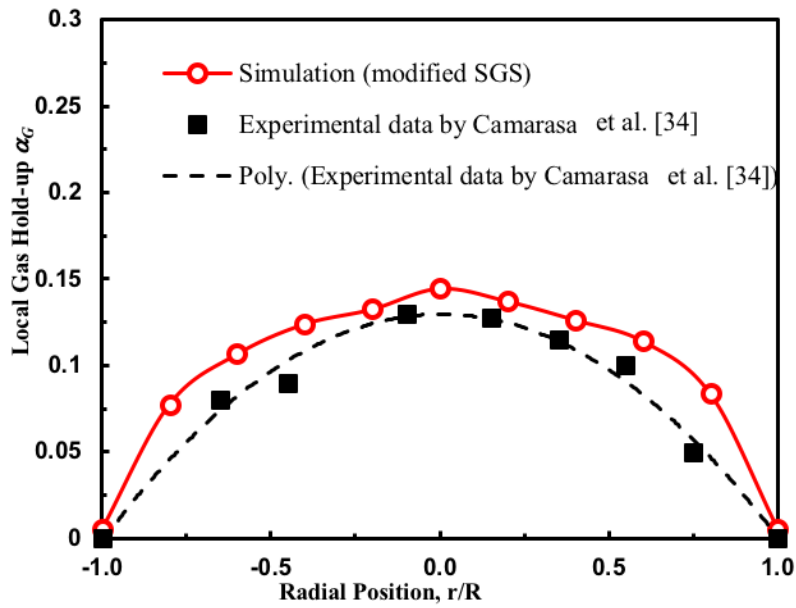


Figure 6. Time-averaged radial distribution of gas hold-up at $H/D = 6$.

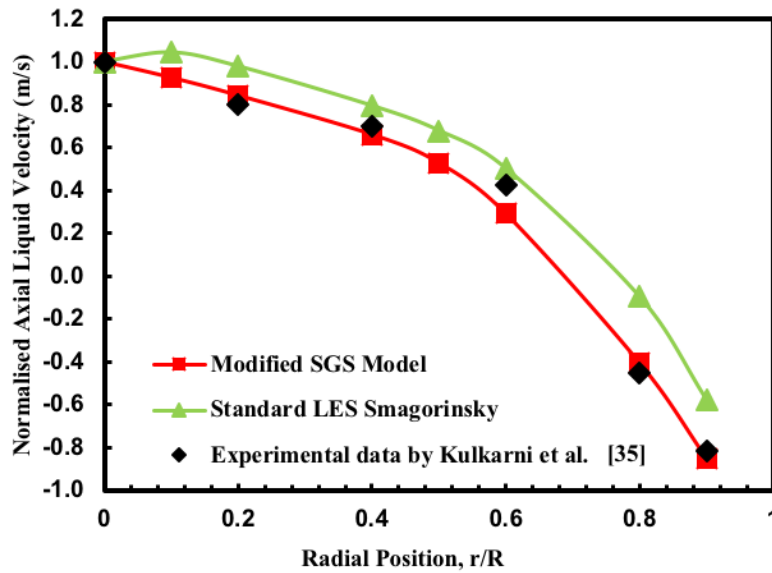


Figure 7. Time-averaged axial liquid velocity at $H/D = 2$.

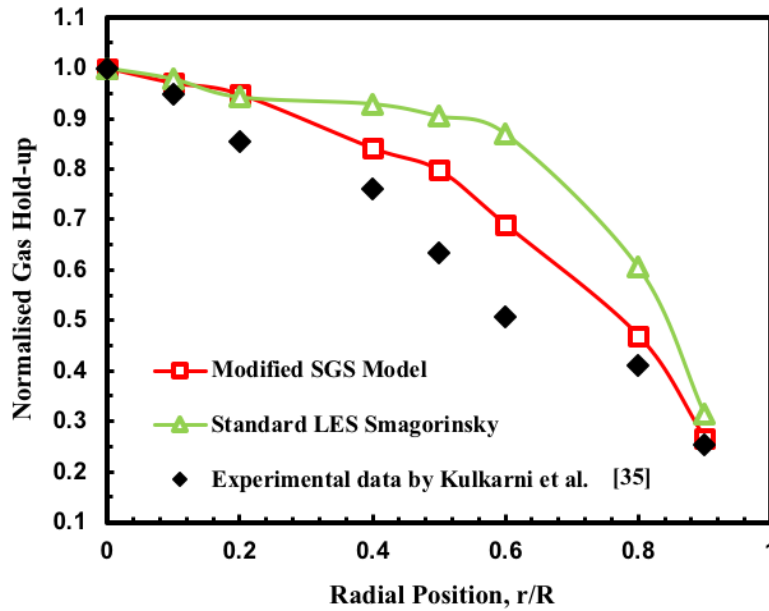


Figure 8. Time-averaged radial distribution of gas hold-up at $H/D = 2$.

In order to further demonstrate the reliability of our modified SGS model, the quantitative comparison between the LES results and the experimental results from Kulkarni *et al.* [35] is also made. In their experimental work, Kulkarni *et al.* settled the measurement points radially at the height of 0.3 m, corresponding to $H/D = 2$. It is expected that the flow field may still be not fully developed and would be influenced by the gas inlet condition. In fact, the air was introduced by a sintered plate in their experiments, which may cause uniform gas inlet distribution. The normalised axial liquid velocity and the gas hold-up against the radial position at $H/D = 2$ obtained from our LES with the modified SGS model are shown in Figures 7 and 8. It can be seen from the figures that generally good agreements with the experimental data were still achieved, clearly indicating the suitability of the modified SGS model.

3.3 Turbulent kinetic energy contributed by shear turbulence and bubble induced turbulence characterized by LES with the modified SGS model

The liquid axial velocity-time series between 50 s and 100 s at the centre of $H/D = 6$, obtained by the modified SGS LES is shown in Figure 9. For comparison purpose, the experimental time-dependent liquid axial velocity sampled corresponding to the same location but acquired by

Kulkarni et al. [35] is also plotted in the figure. It needs to be noted here that the experimental data obtained by Kulkarni *et al.* [35] covering a period of 50 s has 8192 sample points while the results of the modified SGS LES have adopted 10,000 sample points. The LES simulation has reasonably recapture the transient fluctuations as exhibited by the experiment, even the amplitudes of the fluctuations predicted by the modified SGS LES are also consistent with the experimental ones. The observed differences are likely caused by the different sampling rates and the unavoidable noise from the bubble detection in the experiment. As discussed in Kulkarni’s work, since it is not guaranteed that all the bubbles pass entirely and centrally through the measurement volume, the chordal passage will cause refraction on bubbles that eventually lead to the relative higher amplitude liquid velocity [35]. Thus, the probability density function (PDF) and turbulent kinetic energy spectral analysis relating to the time-dependent liquid velocities would be able to provide the physical insight into bubble induced turbulence in the bubble column.

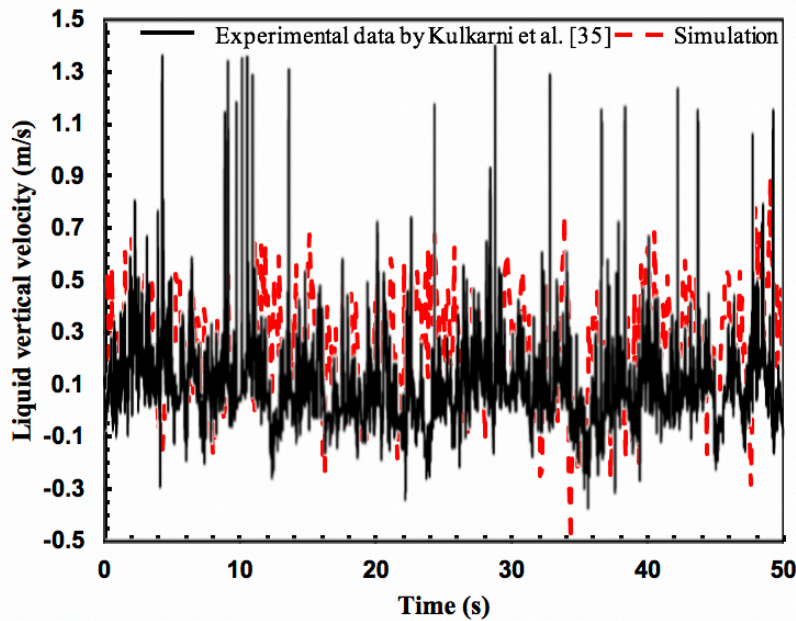


Figure 9. Instantaneous axial velocity-time series.

Figure 10 presents the standardised PDFs for the axial liquid velocity calculated from the simulations for single phase flow, bubbly flow employed modified eddy viscosity model and standard Smagorinsky SGS model. The PDFs of the standardised velocity $(\tilde{u}_i - \bar{\tilde{u}}_i)/\tilde{u}_{i,rms}$ are presented. The PDF of liquid velocity based on a single-phase turbulent flow at a superficial liquid velocity of 0.03162 m/s is presented as the reference, which is nearly distributed as Gaussian

statistics. It is observed from Figure 10, the liquid velocity PDFs for the gas-liquid two-phase flow in the bubble column are asymmetric and show deviation from the single-phase flow's Gaussian behavior with a tail. The occurrence of positive tails have been shown to be caused by the wake behind the rising bubbles and, hence, a larger probability of upward fluctuations [37-40]. Compared with the Smagorinsky SGS model without modification, the relative longer as well as higher positive tails of liquid velocity obtained from the modified SGS model clearly may indicate that the transient behaviour of the bubbles' response to eddies has been captured. It is noted here that the fluctuation caused by the bubbles' response to the turbulent eddies of the similar size with the bubble diameter has been taken into account in the modified SGS model.

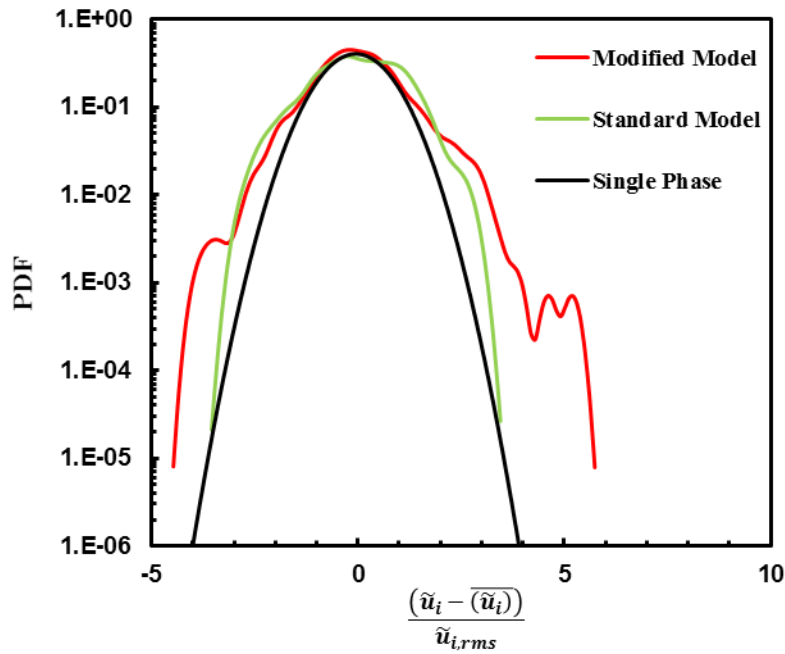


Figure 10. PDFs of the liquid velocity normalized by the RMS velocity.

Regarding to the turbulent kinetic energy of the liquid phase, the LES-filtered power energy spectrum $E(\kappa)$ of the axial turbulent velocity fluctuation obtained at the middle point in the line across the bubble column at $H/D = 6$ are presented in Figure 11(a) and 11(b). The power spectrum is obtained by taking the Fast Fourier Transform (FFT) of the time correlation of axial turbulent velocity fluctuations using the Welch method [41]. Figure 10(a) also presents the one-dimensional spectrum of single phase flow in accordance with Pope's model [42]. The model is described as

$$E_{11}(\kappa) = C_0 \varepsilon^{\frac{2}{3}} \kappa^{-\frac{5}{3}} \left(\frac{\kappa L}{\sqrt{(\kappa L)^2 + C_L}} \right)^{\frac{5}{3} + p_0} \exp \left(-\beta \left([(\kappa_1 \eta)^4 + C_\eta^4]^{\frac{1}{4}} - C_\eta \right) \right) \quad (25)$$

where L and η stand for integral and Kolmogorov length scale, respectively, and the model constants are $C_0 = 0.49$, $p_0 = 0$ for a $-5/3$ spectral slope by default, $C_L = 6.78$, $C_\eta = 0.4$, and $\beta = 5.2$ [43]. As shown in Figure 11(a), the turbulent kinetic energy spectrum predicted by the modified SGS model follows Pope's model well and the modified SGS LES model captures $-5/3$ scaling in the inertial subrange and recovers -3 scaling laws for the wave number greater than the typical wave number characterized by the bubble size, i.e. $\kappa_B = 2\pi/d_B$. It is interesting to note here that the representative bubble frequencies, estimated by $f_B = |\mathbf{u}_G - \mathbf{u}_L|/2\pi d_B$, is 12 Hz when the bubble diameter is 4 mm [44]. In general wave equations, $\kappa = \frac{2\pi}{\lambda} = \frac{2\pi\nu}{u}$, where ν is the frequency of the wave, λ is the wavelength and u is the mean liquid velocity [37]. Thus f_B can be converted to $\kappa_{B1} = 302.80\text{m}^{-1}$. It can be observed from Figure 10(a) that the transition of the $E_{11}(\kappa)$ takes place at $\kappa_{B2} \approx 270 \text{ m}^{-1}$ ($f \approx 10.70$ Hz) where the left of $\kappa_{B2} = 270 \text{ m}^{-1}$ demonstrates the $-5/3$ slope, while the right demonstrates the -3 scaling. This indicates that the turbulent kinetic energy is fed into the liquid with the bubbles' contribution at frequencies around $f = 10.70$ Hz, which is close to the representative bubble frequency. Lance and Bataille [45] have indicated that the eddies induced by bubble wake are very quickly dissipated by viscosity before turbulence spectral transfer can take place. Pope also stated that the directional information of the large scales is missing with the energy passing down the cascade. In the energy cascade ($1 < l_{EI}$), the dominant process is composed of the energy transfer to successively smaller scales and viscous dissipation. Here, l_{EI} is the turbulence length scale between the anisotropic large eddies and the isotropic small eddies, which is hypothesised by Kolmogorov [46]. Thus, the input energy of bubbles will not take part in large length scales, which correspond to low wave numbers, but make a contribution towards higher wave numbers. The production of eddies with the size of the bubbles will contribute towards the dissipation in the higher frequency range as indicated by Lance and Bataille [45]. Since the bubble induced turbulence dissipation can be estimated by $\nu E(\kappa)\kappa^3$, the drag force acting on the gas phase in the turbulent bubbly flow in the bubble column is roughly balanced by the bubble buoyancy on average and one can have the following estimation, given by

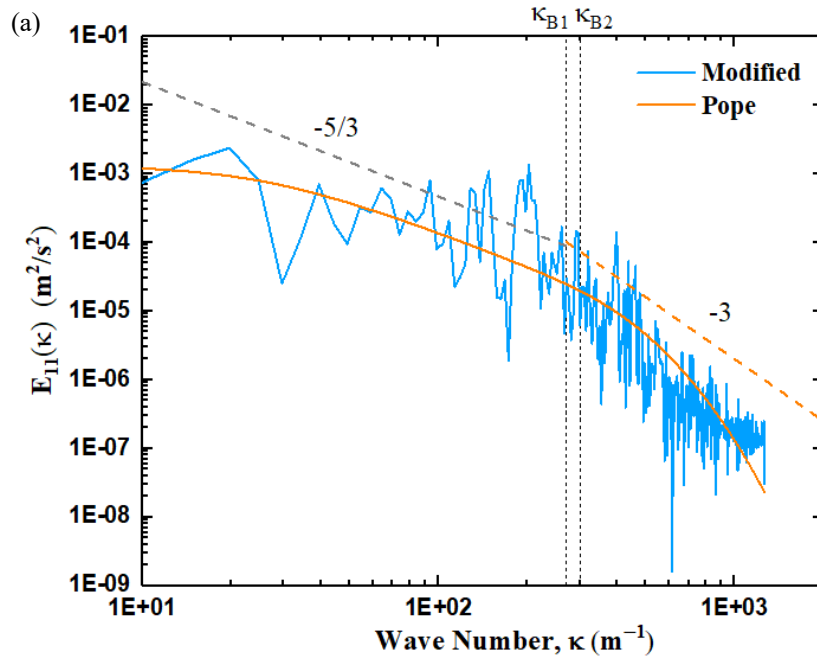
$$\nu E(\kappa)\kappa^3 \sim C_B \alpha_G \left[\frac{3}{4} \frac{C_D}{d_B} (u_B - u_L)^2 \right] |\mathbf{u}_G - \mathbf{u}_L| \quad (26)$$

This leads to $E(\kappa) \sim \kappa^{-3}$, which is also demonstrated by the existing experimental work as well as

DNSs and consistent with our LES results as shown in Figure 10 [47-55]. Based on the modelling discussion, it can be assumed that the total turbulent dissipation rate ε_L is consisted of the turbulent dissipation rate due to shear turbulence and the dissipation due to the bubble-eddy interaction as described by Equation (27), viz.

$$\varepsilon_L = \varepsilon + \varepsilon_B = \varepsilon \left(1 + C_b \overline{\alpha_G} \frac{\lambda}{d} \left(\frac{1}{1+St_{SGS}} \right)^{\frac{3}{2}} \right) = 2\nu \int_0^\infty \kappa^2 E(\kappa) d\kappa \quad (27)$$

The difference in the power spectrum for different SGS models is noted in Figure 11(b). The higher magnitude of $E_{11}(\kappa)$ in $\kappa > \kappa_B$ predicted by the modified SGS model may be caused by the eddy viscosity estimation that considers the bubbles response to eddies. The modified eddy viscosity model takes the competitive fluctuation velocity in the sub-grid scale between bubbles and eddies into account, which is absolutely neglected by the standard LES SGS model. Thus, the energy fed in the system by bubbles are more comprehensively described, leading to a steeper slope when $\kappa > \kappa_B$ in direct cascade, and the slope is much closer to the -3 scaling law compared with the standard model.



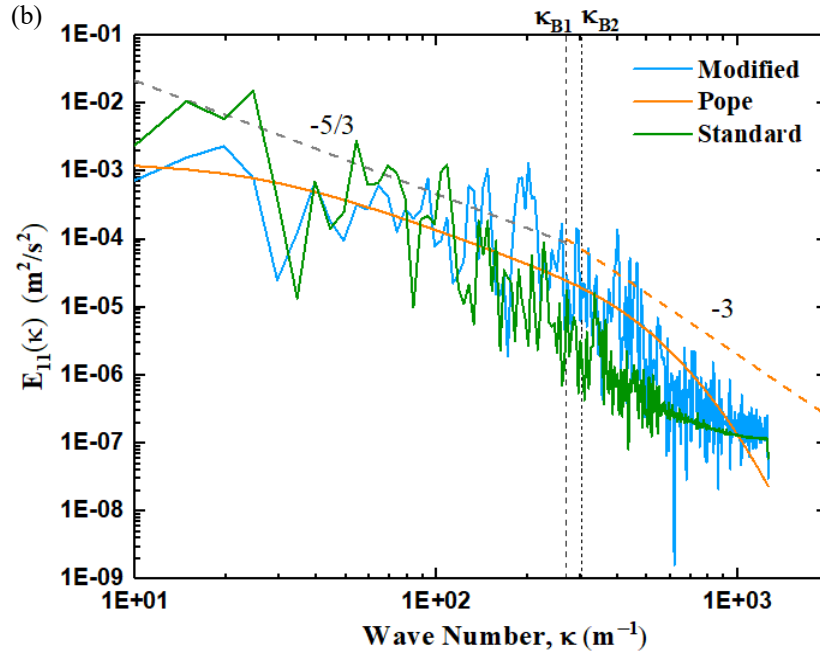


Figure 11. Turbulent kinetic energy spectrum of liquid axial velocity fluctuation, calculated along the centerline at $H/D = 6$. (a) Modified Model; (b) Comparison between Modified and Standard Smagorinsky SGS model.

3.4 Correlation between large eddy structures and local gas holdup

The present study has adopted the vorticity to characterise the large eddy behaviour in the bubble column, defined as the curl of the flow velocity field by $\boldsymbol{\omega} = \nabla \times \mathbf{u}_L$.

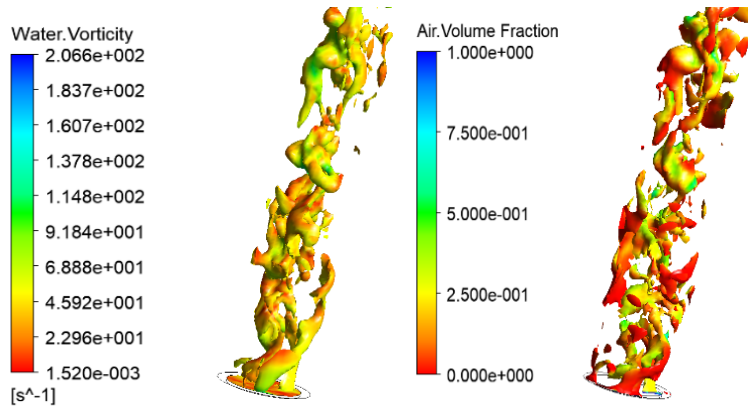


Figure 12. Isosurface of (a) $\alpha_G = 0.23$ highlighted by water vorticity (b) $|\boldsymbol{\omega}_L| = 58 \text{ s}^{-1}$ highlighted by air volume fraction at $t = 90 \text{ s}$.

It is expected that the large eddy structure development in the bubble column would be significantly affected by the entrained bubbles while this interaction between bubbles and turbulent

eddies has been accounted for in the modified SGS model. Thus, a correlation to reflect this coupling can be presented. Figure 12 shows the isosurface of $\alpha_G = 0.23$ highlighted by the vorticity and $|\omega_L| = 58 \text{ s}^{-1}$ highlighted by air volume fraction at $t = 90 \text{ s}$. It can be observed that the bubble volume fraction is strongly coupled with the vorticity. We propose the following spatial correlation between local gas hold-up and vorticity magnitude to characterize the variation of such correlation along the axial height of the bubble column, defined as

$$R(\Delta h) = \frac{|\omega'(h_0)|\alpha'_G(h_0+\Delta h)}{\sqrt{|\omega'^2(h_0)|}\sqrt{\alpha'^2_G(h_0)}} \quad (28)$$

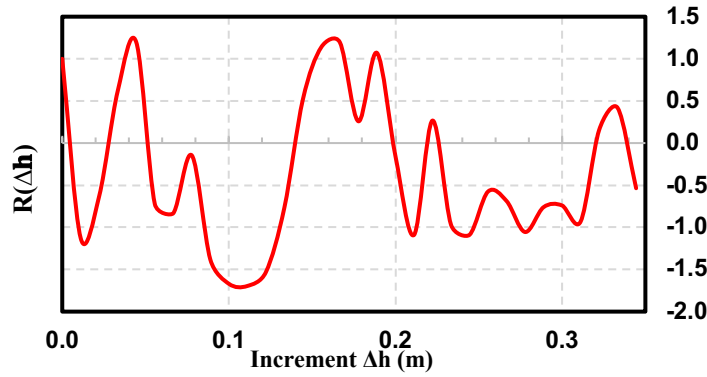


Figure 13. Spatial correlation coefficient $R(\Delta h)$ at $t = 90 \text{ s}$.

Figure 13 presents the spatial correlation coefficient $R(\Delta h)$ along the centerline at different axial height from 0 to 0.35m. As shown in Figure 13, three large peaks are clearly shown in the correlation against the different axial height of the bubble column in the ranges of 0.025-0.05, 0.14-0.2 and 0.32-0.34 m, indicating a strong bubble clustering with the large eddies. It is also noted that the peak of the correlation coefficient of the third one is relatively lower than the first two. This may be explained by the change in the axial height along the column where the large eddies are oscillating. In the range of 0.32-0.34 m, the weaker fluctuation indicates that the typical fluctuated large eddy size may be smaller, entrapping fewer numbers of bubbles. Thus, the value of correlation for the third peak becomes smaller, supported by the predicted $\sqrt{\alpha'^2_G(h_0)}$ being always positive along the axial height. A positive value of the spatial correlation coefficient indicates that the vorticity carried by the large eddies strongly affect the bubble motion and thus, the gas hold-up. Figure 14 displays the cross-section averaged gas hold-up superimposed by the

correlation coefficient distribution. As the combination shown in Figure 14, the occurrence of high gas hold-up is accompanied by the presence of a high spatial correlation coefficient.

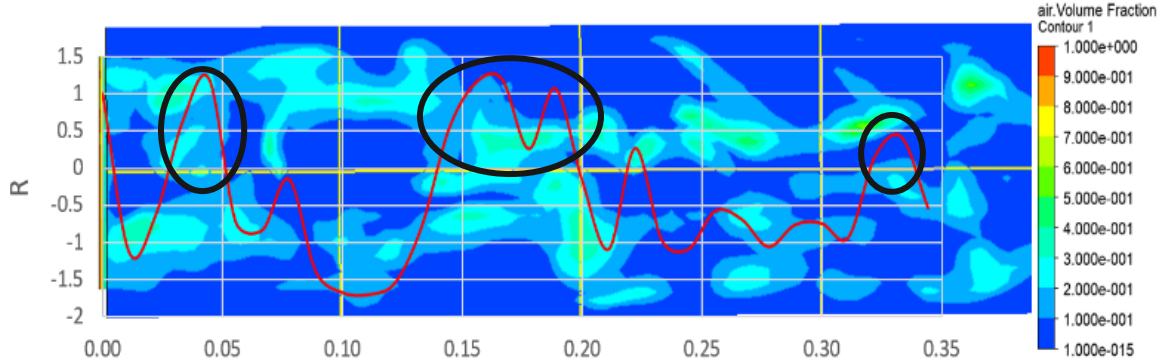


Figure 14. Combination of instantaneous gas hold-up and spatial correlation coefficient at $t = 90s$.

3.5 Interfacial mass transfer across bubbles using the modified SGS model

The volumetric mass transfer coefficient $k_L a$ is an important parameter to evaluate the efficiency of interfacial mass transfer. Besides, when employing the species transport equation to find the species concentration, the contribution from the interfacial mass transfer across the bubbles of the source terms can be calculated with the presence of $k_L a$ [56]. As the spherical bubble assumption was made in the present work, the interfacial area concentration a for the bubbles in the bubble column can be estimated by

$$a = \frac{6\bar{\alpha}_B}{d_B} = \frac{6}{d_B V} \int_V \alpha_g dV \quad (29)$$

where $\bar{\alpha}_B$ is the bubble column volumetric averaged gas holdup. Thus, the coefficient of mass transfer k_L and the interfacial area concentration can be obtained individually from various models of mass transfer. Since the modified SGS model that taking the turbulence kinetic energy contribution from BIT and bubble interaction with the turbulence eddies into account, the relative velocity between gas and liquid and energy dissipation rate play significant roles in estimating the value of interfacial mass transfer coefficient k_L . The eddy cell model was reported by Lamont and Scott [57] and indicated that the very small scale of the turbulent eddies play significant roles in

mass transfer and these motions lead to a sophisticate viscosity, once these small scale behaviors can be controlled and the surface renewal rate as well as the mass transfer mechanism can be then defined analytically and shown as,

$$k_L \propto D_L^{1/2} \left(\frac{\varepsilon_L}{\nu} \right)^{1/4} \quad (30)$$

where D_L is liquid mass diffusivity of liquid phase, ε_L is the turbulence dissipation rate. It can be figured out that k_L can be estimated based on the eddy cell model through a key parameter, turbulence dissipation rate ε_L . The influences of the eddies induced by the bubble wakes and bubbles' dynamic responses to the surrounding liquid on the liquid turbulent kinetic energy spectrum were illustrated in Figure 10. Therefore, apart from the consideration of the simply shear turbulent dissipation, the effect of the interactions between bubbles and eddies is also needed to be addressed. After substituting Equation (27) into Equation (30) yields the estimation for k_L based on the eddy cell model can be expressed as.

$$k_L \propto D_L^{1/2} \left(\frac{\varepsilon \left(1 + C_b \frac{\lambda}{\alpha_G d} \left(\frac{1}{1 + St_{SGS}} \right)^{\frac{3}{2}} \right)}{\nu} \right)^{1/4} \propto D_L^{1/2} \left(\frac{2\nu \int_0^\infty \kappa^2 E(\kappa) d\kappa}{\nu} \right)^{1/4} \quad (31)$$

Equation (31) shows that k_L is related to the kinetic energy integrated from the energy spectrum obtained in Section 3.3. In addition, the assumption can be reasonably made that the mass transfer between the bubbles and the eddies of the similar size or marginally larger is dominant in whole process.

As shown in Figure 15(b), a higher volumetric mass transfer coefficient seems to be more likely in the vicinity of the column wall when implementing the SGS model without considering bubble response to turbulent eddies. However, when the eddy size is slightly larger than the bubble and in the inertial subrange, the bubbles will be strongly entrained by eddies. This phenomenon is well demonstrated by Figure 15(a), where the volumetric mass transfer coefficient is more uniformly distributed compared to the SGS model without modification. Therefore, by employing the modified SGS model, the distribution behavior of mass transfer characterized by $k_L a$ inside the

bubble column can be better analyzed.

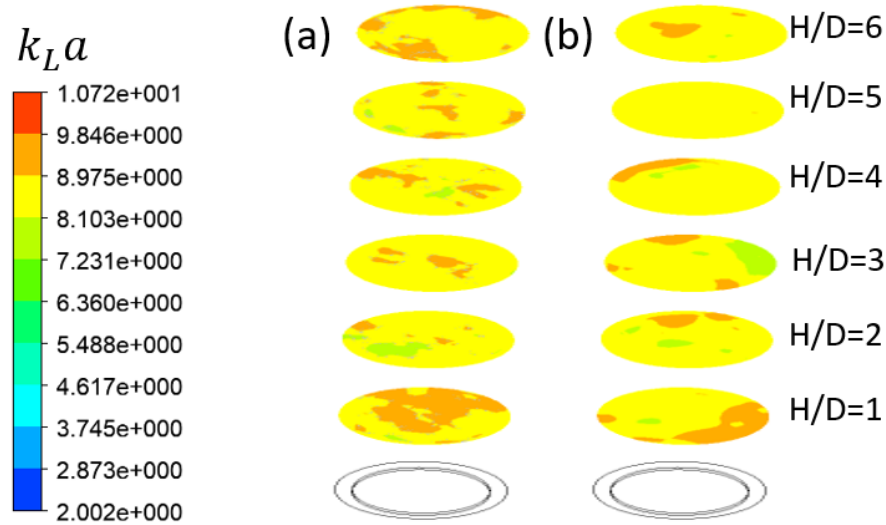


Figure 15. Estimated volumetric mass transfer coefficient at different axial height for (a) modified SGS model (b) SGS model without modification.

4. Conclusions

LES Simulation of gas-liquid flow in a bubble column reactor has been carried out using the modified SGS model, which has taken the bubble-eddy interaction into account. The results of LES simulations clearly indicate that by employing the modified SGS model with consideration of Stokes number, the bubble entrainment transient behaviour in the cylindrical bubble column that was observed in experimental work can be reasonably captured. The effect of the modified SGS model on the velocity profile and gas hold-up is also demonstrated by the simulation. The main conclusions reached as a result of the present study can be summarised as follows:

- (1) It can be observed from the simulation resulting from the modified SGS model that the gas hold-up and velocity profiles demonstrate a better agreement overall with the experimental results [34,35] compared with the standard Smagorinsky SGS model, but both gas hold-up and the streamwise gas velocity are slightly over-predicted in the vicinity of the bubble column wall.
- (2) The use of the modified SGS turbulence model is able to capture the detailed flow behaviour of bubbly flow in the bubble column.
- (3) The power turbulent kinetic energy spectrum of the axial liquid velocity indicates that the slope of classical -5/3 law can still be observed for the frequency range of $f < 10.70$ Hz, followed

approximately by a -3 scaling law when the frequency $f > 10.70$ Hz, the representative bubble frequency calculated according to $f_B = |\mathbf{u}_G - \mathbf{u}_L|/2\pi d_B$ is 12Hz. This is consistent with the recent findings on the bubble induced turbulence as reported by Prakash *et al.* [44], Bouche *et al.* [47], Mendex-diaz *et al.*[48], Mercado *et al.* [49], Murai *et al.*[50], Riboux *et al.* [51, 53], Bunner and Tryggvason[52], Roghair *et al.* [54] as well as Sugiyama *et al.* [55], indicating that the slope of -3 law has been also recovered by using the modified SGS LES for the bubble column.

(4) The spatial correlation between the cross-sectional averaged gas hold-up and local vorticity clearly indicates that the bubbles rising-up is strongly entrained by large spirally turbulent eddies with the trend of bubbles to cluster in the central region of the bubble column.

(5) Based on the eddy cell theory, the volumetric mass transfer coefficient estimated by using the modified SGS model can have better accuracy of estimation of the interfacial mass transfer between bubbles and liquid than that using the standard SGS model.

Acknowledgements

This work was financially supported by the National Natural Science Foundation of China (Grant Nos. 21761132026, 91534118,). Shanshan Long would also acknowledge the support of a full PhD scholarship of University of Nottingham Ningbo China.

Nomenclature

A	[m ²]	Area
C _{AM}	[-]	Virtual mass coefficient
C _D	[-]	Drag coefficient
C _L	[-]	Lift force model constant
C _S	[-]	Sub-grid scale model constant
C _{TD}	[-]	Turbulent dispersion coefficient
D	[m]	Bubble column diameter
d	[m]	Bubble diameter
\bar{D}	[m ² /s]	Mass diffusivity
d	[m]	Bubble diameter
E ₀	[-]	Eötvös number
M _D	[N/m ³]	Drag force

M_L	[N/m ³]	Lift force
M_{AM}	[N/m ³]	Added mass force
M_{TD}	[N/m ³]	Turbulence dispersion force
\mathbf{g}	[m/s ²]	Gravity acceleration
H	[m]	Distance from the bottom surface
K_L	[m/s]	Convective mass transfer film coefficient
Re	[-]	Reynolds number
S	[s ⁻¹]	Characteristic filtered rate of strain
St	[-]	Stokes number
Sc	[-]	Schmidt number
\mathbf{u}	[m/s]	Grid scale velocity vector
$\tilde{\mathbf{u}}$	[m/s]	Instantaneous velocity
\mathbf{u}'	[m/s]	Instantaneous velocity
t	[s]	Time
U_{Slip}	[m/s]	Slip velocity

Greek letters

α	[-]	
ε	[m ² /s ³]	Turbulence dissipation rate
ρ	[kg/m ³]	Fluid density
κ	[m ⁻¹]	Wave number
λ	[m]	Characteristic length scale of eddy
μ	[Pa · s]	Liquid dynamic viscosity
μ_{eff}	[Pa · s]	Effective viscosity of the liquid phase
μ_L	[Pa · s]	Kinematic viscosity
μ_{BI}	[Pa · s]	Bubble induced viscosity
τ	Pa	Shear stress
ν_t	[m ² /s]	Turbulent kinematic viscosity
σ_{TD}	[-]	Turbulent Schmidt number of gas phase
ω	[s ⁻¹]	Water vorticity

Δ	[m]	Filtering width
Δ_i	[m]	Grid spacing in radial direction
Δ_j	[m]	Grid spacing in axial direction
Δ_k	[m]	Grid spacing in lateral direction

Subscripts

B	Bubble
G	Gas phase
L	Liquid phase
k	Either phase
max	Maximum

References

- [1] N.G. Deen , T. Solberg , B.H. Hjertager , Large eddy simulation of the gas–liquid flow in a square cross-sectioned bubble column, *Chem. Eng. Sci.* 56 (21-22) (2001) 6341–6349 .
- [2] D. Lakehal , B.L. Smith , M. Milelli , Large-eddy simulation of bubbly turbulent shear flows, *J. Turbul.* 3 (25) (2002) 1–21 .
- [3] M. Milelli , B.L. Smith , D. Lakehal , Subgrid-scale dynamic modelling in les of turbulent bubbly flows, TSFP Digital Library Online, Begel House Inc., 2001 .
- [4] M.T. Dhotre , B. Niceno , B.L. Smith , Large eddy simulation of a bubble column using dynamic sub-grid scale model, *Chem. Eng. J.* 136 (2-3) (2008) 337–348 .
- [5] F.A. Bombardelli , G.C. Buscaglia , M. García , E.A. Dari , Simulation of bubble plume wandering phenomena in a bubble plume using a k-e model and a large eddy simulation (LES) approach, *Mec. Comput.* 23 (2006) 1969–1994 .
- [6] J. Smagorinsky , General circulation experiments with the primitive equations, *Mon. Weather Rev.* 91 (1963) 99–165 .
- [7] B.L. Smith , M. Milelli , An investigation of confined bubble plumes, in: *Proceedings of the Third International Conference on Multiphase Flow*, 1998, pp. 8–12 . [
- 8] T. Ma , T. Ziegenhein , D. Lucas , J. Fröhlich , Large eddy simulations of the gas–liquid flow in a rectangular bubble column, *Nucl. Eng. Des.* 299 (2016) 146–153 .
- [9] M. Milelli , B.L. Smith , D. Lakehal , Large-eddy simulation of turbulent shear flows laden with bubbles, in: *Direct and Large-Eddy Simulation IV*, Springer, Dordrecht, 2001, pp. 461–470 .
- [10] M. Germano , U. Piomelli , P. Moin , W.H. Cabot , A dynamic subgrid-scale eddy viscosity model, *Phys. Fluids A* 3 (7) (1991) 1760–1765 .

- [11] Y. Sato , M. Sadatomi , K. Sekoguchi , Momentum and heat transfer in two-phase bubble flow—I. Theory, *Int. J. Multiph. Flow* 7 (2) (1981) 167–177 .
- [12] B. Ni čeno , M.T. Dhotre , N.G. Deen , One-equation sub-grid scale (SGS) modelling for Euler–Euler large eddy simulation (EELES) of dispersed bubbly flow, *Chem. Eng. Sci.* 63 (15) (2008) 3923–3931 .
- [13] Z. Liu , B. Li , Scale-adaptive analysis of Euler-Euler large eddy simulation for laboratory scale dispersed bubbly flows, *Chem. Eng. J.* 338 (2018) 465–477 .
- [14] Y. Sato , K. Sekoguchi , Liquid velocity distribution in two-phase bubble flow, *Int. J. Multiph. Flow* 2 (1) (1975) 79–95 .
- [15] F.E. Kruis , K.A. Kusters , The collision rate of particles in turbulent flow, *Chem. Eng. Commun.* 158 (1) (1997) 201–230 .
- [16] S. Lo , D. Zhang , Modelling of break-up and coalescence in bubbly two-phase flows., *J. Computat. Multiph. Flows* 1 (1) (2009) 23–38 .
- [17] Q. Wu , S. Kim , M. Ishii , S.G. Beus , One-group interfacial area transport in vertical bubbly flow, *Int. J. Heat Mass Transf.* 41 (8-9) (1998) 1103–1112 .
- [18] M. Ishii , S. Kim , J. Uhle , Interfacial area transport equation: Model development and benchmark experiments, *Int. J. Heat Mass Transf.* 45 (15) (2002) 3111–3123 .
- [19] X.Y. Fu , M. Ishii , Two-group interfacial area transport in vertical air–water flow-II. Model evaluation, *Nucl. Eng. Des.* 219 (2) (2003) 169–190 .
- [20] W. Yao , C. Morel , Volumetric interfacial area prediction in upward bubbly two-phase flow, *Int. J. Heat Mass Transf.* 47 (2) (2004) 307–328 .
- [21] M. Ishii , S. Kim , J. Kelly , Development of interfacial area transport equation, *Nucl. Eng. Technol.* 37 (6) (2005) 525–536 .
- [22] Y. Liao , T. Ma , L. Liu , T. Ziegenhein , E. Krepper , D. Lucas , Eulerian modelling of turbulent bubbly flow based on a baseline closure concept, *Nucl. Eng. Des.* 337 (2018) 450–459 .
- [23] M. Milelli , A Numerical Analysis of Confined Turbulent Bubble Plumes, ETH Zurich, 2002 .
- [24] M.T. Dhotre , N.G. Deen , B. Niceno , Z. Khan , J.B. Joshi , Large eddy simulation for dispersed bubbly flows: a review, *Int. J. Chem. Eng.* 2013 (2013) 1–22 .
- [25] M. Ishii , N. Zuber , Drag coefficient and relative velocity in bubbly, droplet or particulate flows, *AIChE J.* 25 (5) (1979) 843–855 .
- [26] I. Zun (1980). The Transverse Migration of Bubbles Influenced by Walls in Vertical Bubbly Flow.
- [27] T.R. Auton , The lift force on a spherical body in a rotational flow, *J. Fluid Mech.* 183 (1987) 199–218 .
- [28] A. Tomiyama , H. Tamai , I. Zun , S. Hosokawa , Transverse migration of single bubbles in simple shear flows, *Chem. Eng. Sci.* 57 (2002) 1949–1958 .
- [29] H.A. Jakobsen , B.H. Sannes , S. Grevskott , H.F. Svendsen , Modeling of vertical bubble-driven flows, *Ind. Eng. Chem. Res.* 36 (1997) 4052–4074 .

- [30] A.D. Burns , T. Frank , I. Hamill , J. Shi , The favre averaged drag model for turbulent dispersion in Eulerian multi-phase flows, Proceeding of the Fifth International Conference on Multiphase Flow, 2004 .
- [31] J. Garcia , Study of the turbulence modulation in particle-laden flows using LES, Annu. Res. Briefs 2001 (2001) 177 .
- [32] M.R. Bhole , J.B. Joshi , D. Ramkrishna , CFD simulation of bubble columns incorporating population balance modeling, Chem. Eng. Sci. 63 (8) (2008) 2267–2282 .
- [33] M. Sommerfeld , M. Muniz , T. Reichardt , On the importance of modelling bubble dynamics for point-mass numerical calculations of bubble columns, J. Chem. Eng. Jpn. 51 (4) (2018) 301–317 .
- [34] E. Camarasa , C. Vial , S. Poncin , G. Wild , N. Midoux , J. Bouillard , Influence of coalescence behaviour of the liquid and of gas sparging on hydrodynamics and bubble characteristics in a bubble column, Chem. Eng. Process. 38 (4-6) (1999) 329–344 .
- [35] A. A. Kulkarni , J.B. Joshi , V.R. Kumar , B.D. Kulkarni , Application of multiresolution analysis for simultaneous measurement of gas and liquid velocities and fractional gas hold-up in bubble column using LDA, Chem. Eng. Sci. 56 (17) (2001) 5037–5048 .
- [36] R.C. Chen , J. Reese , L.S. Fan , Flow structure in a three-dimensional bubble column and three-phase fluidized bed, AIChE J. 40 (7) (1994) 1093–1104 .
- [37] F. Risso , K. Ellingsen , Velocity fluctuations in a homogeneous dilute dispersion of high-Reynolds-number rising bubbles, J. Fluid Mech. 453 (2002) 395–410 .
- [38] E. Alm eras , V. Mathai , D. Lohse , C. Sun , Experimental investigation of the turbulence induced by a bubble swarm rising within incident turbulence, J. Fluid Mech. 825 (2017) 1091–1112 .
- [39] F. Risso , Agitation, mixing, and transfers induced by bubbles, Annu. Rev. Fluid Mech. 50 (2018) 25–48 .
- [40] C.C.K. Lai , B. Fraga , M. Dodd , R. Chan , Energy cascade in a homogeneous swarm of bubbles rising in a vertical channel, in: Proceedings of the Summer Program, 2018, Centre for Turbulence Research, 2018, pp. 55–64 .
- [41] P. Welch , The use of fast Fourier transform for the estimation of power spectra: a method based on time averaging over short, modified periodograms, IEEE Trans. Audio Electroacoust. 15 (2) (1967) 70–73 .
- [42] S.B. Pope , Turbulent Flows, Cambridge University Press, 2001 .
- [43] C.C. Lai , S.A. Socolofsky , The turbulent kinetic energy budget in a bubble plume, J. Fluid Mech. 865 (2019) 993–1041 .
- [44] V.N. Prakash , J.M. Mercado , L. van Wijngaarden , E. Mancilla , Y. Tagawa , D. Lohse , C. Sun , Energy spectra in turbulent bubbly flows, J. Fluid Mech. 791 (2016) 174–190 .
- [45] M. Lance , J. Bataille , Turbulence in the liquid phase of a uniform bubbly air–water flow, J. Fluid Mech. 222 (1991) 95–118 .

- [46] A.N. Kolmogorov , The local structure of turbulence in incompressible viscous fluid for very large Reynolds numbers, *Proc. R. Soc. Lond. Ser. A: Math. Phys. Sci.* 434 (1890) (1991) 9–13 .
- [47] E. Bouche , V. Roig , F. Risso , A.M. Billet , Homogeneous swarm of high-Reynolds-number bubbles rising within a thin gap. Part 2. Liquid dynamics, *J. Fluid Mech.* 758 (2014) 508–521 .
- [48] S. Mendez-Diaz , J.C. Serrano-Garcia , R. Zenit , J.A. Hernandez-Cordero , Power spectral distributions of pseudo-turbulent bubbly flows, *Phys. Fluids* 25 (4) (2013) 043303 .
- [49] J.M. Mercado , D.C. Gomez , D. Van Gils , C. Sun , D. Lohse , On bubble clustering and energy spectra in pseudo-turbulence, *J. Fluid Mech.* 650 (2010) 287–306 .
- [50] Y. Murai , A. Kitagawa , X.Q. Song , J. Ohta , F. Yamamoto , Inverse energy cascade structure of turbulence in a bubble flow: numerical analysis using Eulerian-Lagrangian model equations, *JSME Int. J. Ser. B Fluids Therm. Eng.* 43 (2) (2000) 197–205 .
- [51] G. Riboux , F. Risso , D. Legendre , Experimental characterization of the agitation generated by bubbles rising at high Reynolds number, *J. Fluid Mech.* 643 (2010) 509–539 .
- [52] B. Bunner , G. Tryggvason , Effect of bubble deformation on the properties of bubbly flows, *J. Fluid Mech.* 495 (2003) 77–118 .
- [53] G. Riboux , D. Legendre , F. Risso , A model of bubble-induced turbulence based on large-scale wake interactions, *J. Fluid Mech.* 719 (2013) 362–387 .
- [54] I. Roghair , J.M. Mercado , M.V.S. Annaland , H. Kuipers , C. Sun , D. Lohse , Energy spectra and bubble velocity distributions in pseudo-turbulence: Numerical simulations vs. experiments, *Int. J. Multiph. Flow* 37 (9) (2011) 1093–1098 .
- [55] K. Sugiyama , S. Takagi , Y. Matsumoto , Multi-scale analysis of bubbly flows, *Comput. Methods Appl. Mech. Eng.* 191 (6-7) (2001) 689–704 .
- [56] W. Shi , J. Yang , G. Li , Y. Zong , X. Yang , Modelling of bubbly flow in bubble column reactors with an improved breakup kernel accounting for bubble shape variations, *Heat and Mass Transfer: Advances in Modelling and Experimental Study for Industrial Applications*, 65, InTechOpen, 2018 .
- [57] J.C. Lamont , D.S. Scott , An eddy cell model of mass transfer into the surface of a turbulent liquid, *AIChE J.* 16 (4) (1970) 513–519 .
- [58] M.H. Mohammadi , F. Sotiropoulos , J.R. Brinkerhoff, Eulerian-Eulerian large eddy simulation of two-phase dilute bubbly flows, *Chem. Eng. Sci.* 208 (2019) 115–156 .
- [59] L. Zhao , M.C. Boufadel , K. Lee , T. King , N. Loney , X. Geng , Evolution of bubble size distribution from gas blowout in shallow water, *J. Geophys. Res.: Oceans* 121 (3) (2016) 1573–1599 .